Spacetime Frequency-Multiplexed Digital-RF Array Receivers with Reduced ADC Count

Najath Akram, *Member, IEEE,* Viduneth Ariyarathna, *Member, IEEE,* Soumyajit Mandal, *Senior Member, IEEE,* Leonid Belostotski, *Senior Member, IEEE,* Theodore S. Rappaport, *Fellow, IEEE,* and Arjuna Madanayake, *Member, IEEE*

***Abstract*—Wireless systems operating at mm-wave frequencies require dense antenna arrays to achieve directional gain for overcoming high path loss. Digital mm-wave arrays retain spatial degrees of freedom, but require a dedicated analog to data converter (ADC) per spatial channel, leading to undesirably high receiver complexity, large ADC count, and power consumption. This paper exploits directional sparsity to reduce the number of receivers and ADCs with minimal loss in performance. A multidimensional (MD) linear transformation using transmission lines and a K:1 combiner is used to reduce the number of ADCs by a factor K. Simulations verify that the proposed method can lead to better than 50% ADC complexity reductions (for $K \geq 2$) for linear arrays and more than 75% ADC complexity reduction (for $K \geq 4$) for rectangular arrays when sparsity conditions are met. Unlike in analog-digital hybrid beamforming, where a phased-array combines K channels to a single ADC, the proposed method does not lead to loss of spatial degrees of freedom.**

***Index Terms*—Multidimensional signal processing, phased arrays, analog-digital conversion.**

I. Introduction

Advances in radio frequency (RF) technology have enabled wireless systems, such as 5G/6G networks, to occupy higher frequency bands in the mm-wave regime, thus facilitating faster throughput and increased network capacity [1], [2]. The reduced physical size of high-frequency antennas makes it possible to pack more antennas in a given aperture. Therefore, mm-wave wireless systems can compensate for high path loss by introducing multiple antenna elements without increasing the total physical size of the array [3]. As a result, linear and rectangular antenna arrays are becoming increasingly common in emerging mm-wave and sub-THz wireless systems.

Here we focus on receive-mode arrays. Each element in such arrays requires an analog front-end consisting of a low-noise amplifier (LNA), band selection filters, downconverting mixer, intermediate frequency (IF) amplifiers, and an anti-aliasing filter. In addition, implementing a maximally-flexible digital beamformer (e.g., to form multiple simultaneous RF beams) requires a wideband ADC for each front-end. In spite of ongoing progress in ADC design, the sheer number of ADCs that are needed for such fully-digital beamformers remains a major bottleneck for emerging systems with a large number of channels/antennas. For example, massive multi-input multi-output (MIMO) 5G systems [4]–[7] and their extensions to the mm-wave and sub-THz regions, such as extremely large aperture arrays (ELAA), holographic massive MIMO, large-scale MIMO radar, and intelligent massive MIMO, may require hundreds or thousands of antenna elements and ADCs packed within a small area [6].

An N–element fully-digital receive array requires N ADCs for a non-zero IF; this number doubles for direct conversion receivers due to the need for I-Q baseband channels. Moreover, certain applications (e.g., weather and aviation radar), require dual-polarized arrays that process both field polarizations [8]–[12]. Using a dedicated converter for each field component thus further increases the ADC count to $2N$ at IF, or $4N$ at baseband. In either case, the overall system complexity, chip/board area, power consumption, and cost of fully-digital arrays is often dominated by that of the wideband ADCs.

Thus, the key bottleneck to further scaling of antenna arrays (which would be beneficial for increasing channel capacity) is the need for a dedicated ADC per antenna element and polarization direction. In our previous work [13], we proposed a partial solution to this problem by combining two polarizations such that the number of ADCs was halved. In this paper, we expand on that work by exploiting sparsity properties of the multi-dimensional (MD) spatio-temporal spectrum to allow the use of only one ADC for $K \geq 2$ RF front-ends. As a result, our approach, which is independent of the modulation scheme and channel characteristics, can reduce the number of ADCs and associated resource/power consumption by at least 50%.

II. Proposed Architecture

A. Review: Key 2-D Spectral Properties

Our analysis focuses on the most common array geometries, namely uniform linear arrays (ULAs) and uniform rectangular arrays (URAs). Consider a wideband uniform plane wave impinging on a ULA with an inter-element spacing of Δx at a direction of arrival (DOA) of ψ, where $(-\frac{\pi}{2} \leq \psi \leq \frac{\pi}{2})$ as shown in Fig. 1(a). The value of Δx is chosen to satisfy the spatial Nyquist sampling criterion. Let the antennas have a directional receive pattern, such that i) the main lobe extends in the broadside direction, and ii) the radiation pattern reduces to

N. Akram and A. Madanayake are with the Department of Electrical and Computer Engineering, Florida International University, Miami, FL 33172, USA. E-mail: akram.m.n@ieee.org, amadanay@fiu.edu.

V. Ariyarathna is with the Department of Electrical and Computer Engineering, Northeastern University, Boston, MA 02115, USA.

S. Mandal is with the Department of Electrical and Computer Engineering, University of Florida, Gainesville, FL 32511, USA.

L. Belostotski is with the Department of Electrical and Computer Engineering, University of Calgary, Calgary, AB T2N 1N4, Canada.

T. S. Rappaport is with NYU Wireless, New York University, Brooklyn, NY 11201, USA.

Manuscript received March 16, 2021.

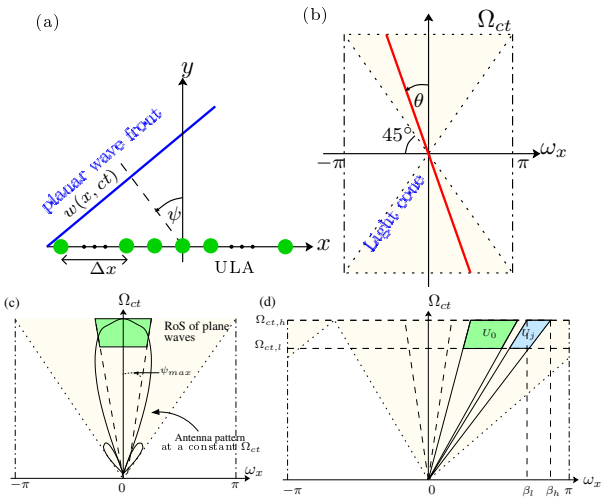

Fig. 1. (a) A plane wave impinging on a ULA; (b) ROS of the plane waves impinging on a ULA in the 2-D frequency domain; (c) positive half (temporal) of the 2-D frequency plane showing the finite-element pattern; (d) illustration of the linear-transformed spectrum using the transformation matrix $\mathbf{V}$.

a pre-determined level (say -10 dB, or 10% power) at angles $\psi = \psi_{max}$. The signal received by each antenna element of the ULA produces a 2-D signal that is discrete in space and continuous in time for a given polarization. Each antenna element uses an ADC with sampling frequency $f_s = 1/(\Delta T)$ to discretize the continuous-time signal, where f_s is chosen to satisfy the temporal Nyquist criterion. Thus the discretized 2-D space-time signal from the digital receive-mode array is:

$$w_{DSDT}(n_x, n_{ct}) = w_s(-n_x \Delta x \sin\psi + c n_{ct} \Delta T). \quad (1)$$

The region of support (ROS) is defined as the part of a Fourier domain where the magnitude of the frequency spectrum is *not defined to be zero*. In the 2-D spatio-temporal frequency domain, the ROS of $W(\omega_x, \omega_{ct})$ is confined to a straight line passing through the origin that makes an angle of θ with the ω_{ct} axis; here $\tan\theta = \sin\psi$ is shown in Fig. 1(b). Also $(\omega_x, \omega_{ct}) \in \mathbb{R}^2$ is the domain of the 2-D frequency spectrum, where ω_{ct} represents the normalized temporal frequency. Since $-1 \leq \sin\psi \leq 1$, the range of θ is constrained by $-1 \leq \tan\theta \leq 1$ such that $-\frac{\pi}{4} \leq \theta \leq \frac{\pi}{4}$. When directional antennas that do not produce signals beyond ψ_{max} are used in the array in place of omni-directional elements, the spectral ROS is further constrained to line-shaped regions that are within the dual-fan bound by $\theta_{max} = \pm\tan^{-1}\sin\psi_{max}$ [14].

B. Introduction to the Proposed Architecture

Practical antennas have constrained radiation patterns that act like spatial low-pass filters (Fig. 1(c)). Element patterns are constrained to the region $-\psi_{max} \leq \psi \leq \psi_{max}$ for a predetermined gain threshold (e.g., -10 dB), such that the gain is much lower than this threshold for $|\psi| > \psi_{max}$ and the resulting 2-D spatio-temporal frequency domain is sparse. The approximately empty space can be utilized to multiplex signals from multiple antenna elements (or polarizations) through a receiver chain, thus reducing the required number of front-ends and ADCs. Such multiplexing occurs at a controlled level of interference that is part of the design trade-off for the

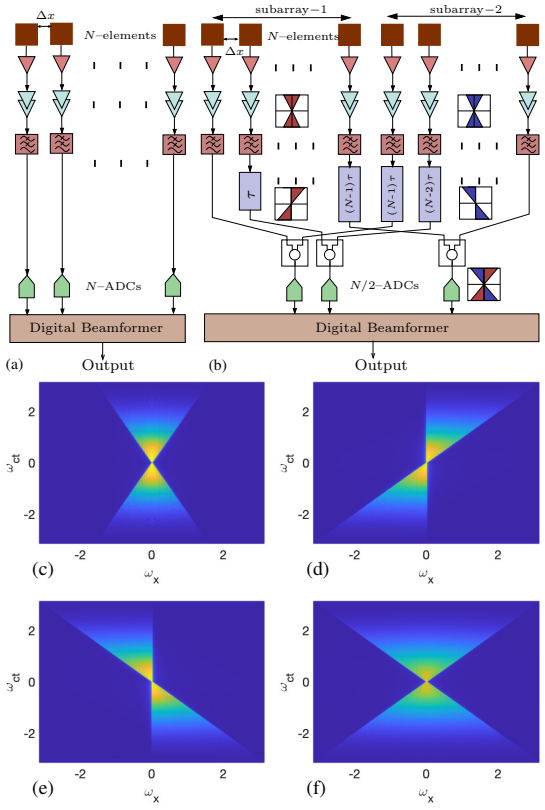

Fig. 2. Architectures for all-digital beamforming arrays: (a) conventional ULA, and (b) MDLT-based ULA, in which linear-transformed spectra are combined to reduce the ADC count. (c) Intact MD spectrum observed by the ULA; linear-transformed spectra for (d) sub-array-1, and (e) sub-array-2. (f) Combined spectrum digitized by the reduced number of ADCs.

system. Mathematically, multiplexing can be achieved using multidimensional linear transforms (MDLTs) to transform the spectra of different sub-arrays to minimally interfering regions of the MD domain of the spatio-temporal Fourier transform.

After the sparse ROS are linear-transformed to lie on (ideally) mutually exclusive regions of the 2-D spectral domain, they can be linearly combined [15] without interference and sampled using one set of ADCs. Finally, the individual signals from the ULA can be recovered using a 2-D digital filter. If the pattern per element (or sub-array) is constrained to be within $\pm\psi_{max} = \pi/2K$ where $K \in \mathbb{Z}^+$, then the number of ADCs can be reduced by a factor of K in the best case scenario.

For example, consider an $N-$element Nyquist-sampled ULA (shown in Fig. 2(a)) where the antenna patterns are restricted to $0 < \psi < \frac{\pi}{6}$, such that the ROS in the MD spectrum is constrained to be within $-\tan^{-1}\frac{1}{2} \leq \theta \leq \tan^{-1}\frac{1}{2}$ as shown in Fig. 2(c). To apply the chosen MDLT, the ULA is divided into two sub-arrays, as shown in Fig. 2(b), without changing the inter-element spacing. The LT shifts the MD spectra of sub-array-1 and sub-array-2 to the left and right respectively (Figs. 2(d)-(e)), such that the signals can be combined without spectral interference (Fig. 2(f)).

C. Mathematical Analysis

If $W_m(\mathbf{\Omega})$ is the mixed domain 2-D Fourier spectrum of the 2-D mixed-domain plane wave denoted as $w_m(\boldsymbol{u})$, $\boldsymbol{\omega} =$

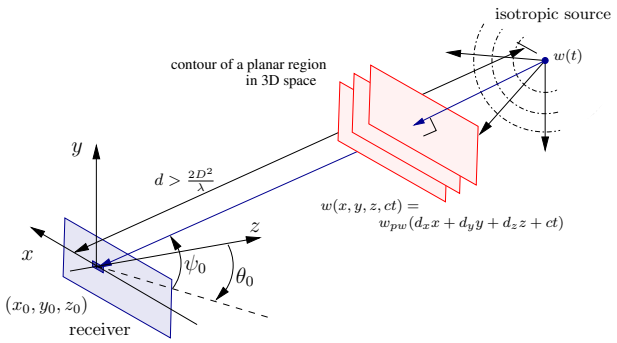

Fig. 3. A plane wave incident on a rectangular aperture in the far field.

$[\omega_x,\ \Omega_{ct}]^\top$, and $\boldsymbol{u} = [n_x,\ ct]^\top$ ($n_x \in \mathbb{Z}$, $ct \in \mathbb{R}$), then the Fourier spectrum of $w_m(\mathbf{V}\boldsymbol{u})$ where $\mathbf{V}$ is an invertible 2×2 square matrix is $\frac{W_m(\mathbf{V}^{-\top}\boldsymbol{\omega})}{|\det\ V|}$ as proven below [16], [17].

Let $x_a(\mathbf{t})$ be a 2-D analog signal where $\mathbf{t} = [t_1, t_2]^\top \in \mathbb{R}^2$, and $\mathbf{V}$ be the sampling matrix made up of linearly independent sampling vectors $\mathbf{v}_1 = [v_{11}, v_{21}]^\top$, $\mathbf{v}_2 = [v_{12}, v_{22}]^\top$, where $\mathbf{V} = [\mathbf{v}_1|\mathbf{v}_2]$. In this case $\mathbf{t} = \mathbf{V}\mathbf{n}$, where $\mathbf{n} = [n_x, ct]^\top$, $n_x \in \mathbb{Z}$, and $ct \in \mathbb{R}$. The spatially-sampled mixed-domain signal is then represented as $x_m(\mathbf{n}) = x_a(\mathbf{V}\mathbf{n})$. The original analog signal $x_a(\mathbf{t})$ satisfies the Fourier relationships $x_a(t) \iff X_a(\omega)$. Letting $\boldsymbol{\zeta} = \mathbf{V}'\boldsymbol{\omega}$, the similar Fourier relationships for the sampled signal $x_m(\mathbf{n})$ are given by

$$X_m(\boldsymbol{\zeta}) = \sum_{n_x}\left[\int_{-\infty}^{+\infty} x_m(\mathbf{n}) e^{-j\Omega_{ct}ct} e^{-j\omega_x n_x} d\Omega_{ct}\right],$$

$$x_m(\mathbf{n}) = \frac{1}{4\pi^2}\int_{-\infty}^{+\infty}\int_{-\pi}^{+\pi} X_m(\boldsymbol{\zeta}) e^{j\Omega_{ct}ct} e^{j\omega_x n_x} d\omega_x d\Omega_{ct}.$$

Since $x_m(\mathbf{n})$ is obtained by sampling $x_a(t)$, we can also write

$$x_m(\mathbf{n}) = x_a(\mathbf{V}\mathbf{n}) = \frac{1}{4\pi^2}\int_{-\infty}^{+\infty} X_a(\boldsymbol{\omega}) e^{j\boldsymbol{\omega}\mathbf{V}\mathbf{n}} d\boldsymbol{\omega}. \quad (2)$$

Substituting $\boldsymbol{\zeta} = \mathbf{V}'\boldsymbol{\omega}$,

$$x_m(\mathbf{n}) = \frac{1}{4\pi^2}\int_{-\infty}^{+\infty}\int_{-\pi}^{+\pi} \frac{1}{|\det \mathbf{V}|}\sum_k X_a(\mathbf{V}^{-\top}(\boldsymbol{\zeta} - 2\pi k\mathbf{e}_1)) e^{j\boldsymbol{\zeta}'\mathbf{n}} e^{-j2\pi k\mathbf{e}_1'\mathbf{n}} d\boldsymbol{\omega}, \quad (3)$$

where $\mathbf{e}_1 = [1\ 0]^\top$, $k \in \mathbb{Z}$, and the last term is unity. Thus,

$$x_m(\mathbf{n}) = \frac{1}{4\pi^2}\int_{-\infty}^{+\infty}\int_{-\pi}^{+\pi} \frac{1}{|\det \mathbf{V}|}\sum_k X_a(\mathbf{V}^{-\top}(\boldsymbol{\zeta} - 2\pi k\mathbf{e}_1)) e^{j(\Omega_x n_x + \Omega_{ct}ct)} d\boldsymbol{\omega}. \quad (4)$$

By comparison with (2), we can see that

$$X_m(\boldsymbol{\zeta}) = \frac{1}{|\det \mathbf{V}|}\sum_k X_a(\mathbf{V}^{-\top}(\boldsymbol{\zeta} - 2\pi k\mathbf{e}_1)).$$

Setting $\mathbf{V} = \begin{bmatrix} 1 & 0 \\ -c\tau & 1 \end{bmatrix}$, i.e., $\mathbf{V}^{-\top} = \begin{bmatrix} 1 & c\tau \\ 0 & 1 \end{bmatrix}$ would enforce a linear transform on the 2-D signal by introducing a $n_x\tau$, $\tau \in \mathbb{R}$ delay to the signal at each spatial sample location n_x; here τ would depend on $\frac{\Delta x \sin\psi_{max}}{c}$. The linearly transformed spectra of $W_m\left(\mathbf{V}^{-\top}\boldsymbol{\omega}\right)$ (corresponding to the original $W_m(\boldsymbol{\omega})$ shown in green in Fig. 1(c)) are shown in Fig. 1(d). For an antenna array receiving a 2-D plane wave, the received signal $s_m(\boldsymbol{u})$ and its spectrum $S_m(\boldsymbol{\omega})$ are filtered by the antenna response where $S_m(\boldsymbol{\omega}) = W_m(\boldsymbol{\omega})\Psi(\boldsymbol{\omega})$ and $\Psi(\boldsymbol{\omega})$ is the radiation pattern in the 2-D Fourier domain.

The antenna pattern provides room for different spectra captured by equi-spaced equi-element sub-arrays to be shifted and combined together, thus reducing the number of required front-end chains. Alternatively, omni antennas may also be used under conditions of constrained field-of-view (FoV) with no strong directional interference outside the expected FoV. For example, radio astronomy arrays may look up at the sky in a 30° FoV, or a long-range radar receiver may sense within a cone of interest. The signal energy of the spectrum $S_m(\boldsymbol{\omega})$ within the frequency band U_l (in Fig. 1(d)) is given by

$$I_{l,0} = \frac{1}{4\pi^2}\int\int_{U_l} \frac{1}{|\det \mathbf{V}|^2}|S_m(\mathbf{V}^{-\top}\boldsymbol{\omega})|^2 d\boldsymbol{\omega}. \quad (5)$$

If U_l is defined by $\omega_x = [\beta_l, \beta_h]$, the corresponding 2D spectral region is defined by the intersection of four lines: $\Omega_{ct} = \Omega_{ct,h}$, $\Omega_{ct} = \Omega_{ct,l}$, $\Omega_{ct} = \frac{\Omega_{ct,h}}{\beta_l}\omega_x$, and $\Omega_{ct} = \frac{\Omega_{ct,h}}{\beta_h}\omega_x$. As a result, (5) can be written as

$$I_{l,0} = \frac{1}{4\pi^2}\int_{\Omega_{ct,l}}^{\Omega_{ct,h}}\int_{\frac{\beta_l\Omega_{ct}}{\Omega_{ct,h}}}^{\frac{\beta_h\Omega_{ct}}{\Omega_{ct,h}}} \frac{1}{|\det \mathbf{V}|^2}|W_m(\mathbf{V}^{-\top}\boldsymbol{\omega}) \Psi(\mathbf{V}^{-\top}\boldsymbol{\omega})|^2 d\boldsymbol{\omega}. \quad (6)$$

D. Extension to K Bands with Different Linear Transforms

Suppose we use different transformations $\mathbf{V}_k = \begin{bmatrix} 1 & 0 \\ -c\tau_k & 1 \end{bmatrix}$, $k \in [0, K-1]$ to transform signals from antenna elements (or sub-arrays of identical spacing and size) in an ULA. The idea is to choose matrices $\mathbf{V}_k$ such that all the K signals $s_{m,k}(\boldsymbol{V}_k\boldsymbol{u})$ are combined to make

$$y_{m,k}(\boldsymbol{u}) = \sum_{k=0}^{K-1} s_{m,k}(\boldsymbol{V}_k\boldsymbol{u}) \quad (7)$$

such that the required ADC complexity can be reduced by a factor of K ($K \in \mathbb{Z}^+$) while also minimizing the interference between different spatial bands. The spectrum of the combined mixed-domain 2D signal after the linear transformation is

$$Y_m(\boldsymbol{\omega}) = \sum_{k=0}^{K-1} S_{m,k}\left(\mathbf{V}_k^{-\top}\boldsymbol{\omega}\right), \quad (8)$$

where $S_{m,k}\left(\mathbf{V}_k^{-\top}\boldsymbol{\omega}\right)$ is the spectrum of the linearly-transformed 2D signal from the kth sub array. Suppose $\mathbf{V}_{k=l}$ is used to transform the signal of the l-th sub-array such that the dominant spectrum of the signal $S_{m,k}\left(\mathbf{V}_l^{-\top}\boldsymbol{\omega}\right)$ is moved to the spatial frequency band U_l. Now the interference energy that is artificially created in the U_l band is calculated as follows:

$$I_l = \frac{1}{4\pi^2}\int_{\Omega_{ct,l}}^{\Omega_{ct,h}}\int_{\frac{\beta_l\Omega_{ct}}{\Omega_{ct,h}}}^{\frac{\beta_h\Omega_{ct}}{\Omega_{ct,h}}} \left|\sum_{\substack{k=0 \\ k\neq l}}^{K-1}\left[\frac{1}{|\det \mathbf{V_k}|}W_{m,k}(\mathbf{V_k}^{-\top}\boldsymbol{\omega})\ \Psi_k(\mathbf{V_k}^{-\top}\boldsymbol{\omega})\right]\right|^2 d\boldsymbol{\omega}. \quad (9)$$

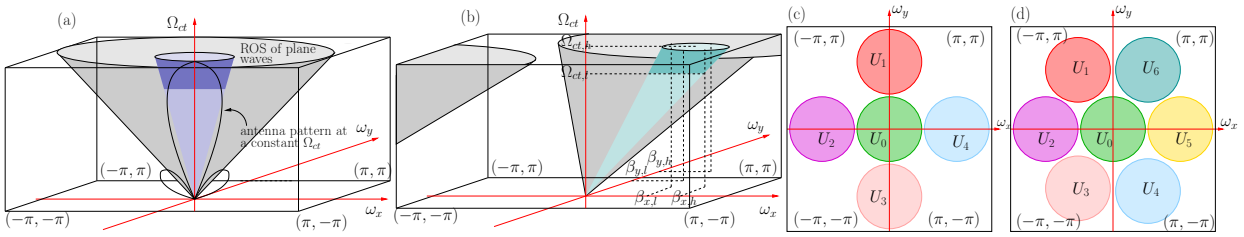

Fig. 4. (a) The spectrum observed by the rectangular aperture, and (b) LT spectrum. Possible LT configurations to combine (c) five, and (d) seven channels.

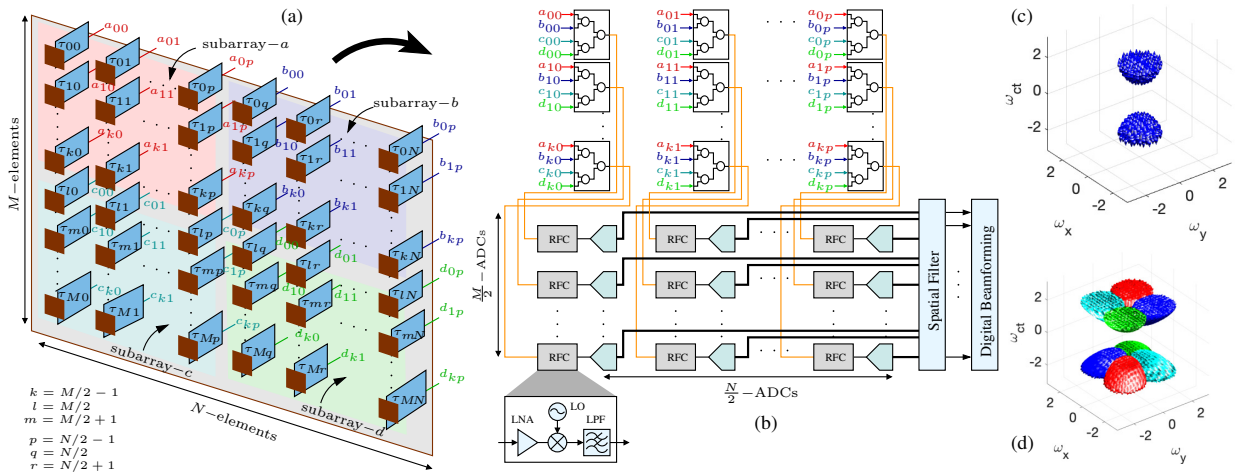

Fig. 5. (a) URA with MD linear transforms at RF, and (b) combination stage [15] followed by RF chains (RFCs) and ADCs for a fully-digital beamformer. Simulated spectra: (c) observed by the rectangular aperture, and (d) linear transformed and combined without interference.

The model in (9) can now be used to derive the distortion introduced by the added signal processing by plugging in analytical or simulated antenna radiation patterns.

E. Extension to Rectangular Apertures

Consider an $N_x \times N_y$ Nyquist sampled rectangular aperture in the far-field shown in Fig. 3. By extending the mathematical analysis to the mixed domain 3-D Fourier spectrum $W_m(\boldsymbol{\omega})$, where the 3-D mixed domain plane wave is denoted as $w_m(\boldsymbol{u})$, $\boldsymbol{\omega} = \left[e^{-j\omega_x},\ e^{-j\omega_y},\ \Omega_{ct}\right]^\top$ and $\boldsymbol{u} = [n_x,\ n_y,\ ct]^\top$ ($n_x, n_y \in \mathbb{Z}$ and $ct \in \mathbb{R}$), the Fourier spectrum of $w_m(\mathbf{V}\boldsymbol{u})$, where $\mathbf{V}$ is an invertible 3×3 square matrix, is $\frac{W_m(\mathbf{V}^{-\top}\boldsymbol{\omega})}{|\det\ V|}$. For $\mathbf{V} = \begin{bmatrix} 1 & 0 & 0 \\ 0 & 1 & 0 \\ -\tau_x & -\tau_y & 1 \end{bmatrix}$, i.e., $\mathbf{V}^{-\top} = \begin{bmatrix} 1 & 0 & \tau_x \\ 0 & 1 & \tau_y \\ 0 & 0 & 1 \end{bmatrix}$, the LT extends to 3-D such that the temporal frequency is unaffected while the spatial frequencies are shifted to

$$\omega'_x = \omega_x + \tau_x\Omega_{ct},\ \omega'_y = \omega_y + \tau_y\Omega_{ct},\ \text{and}\ \Omega'_{ct} = \Omega_{ct}, \quad (10)$$

where τ_x depends on $\frac{\Delta x \sin\theta\cos\psi}{c}$ and τ_y depends on $\frac{\Delta y \sin\theta\sin\psi}{c}$. The transformed mixed-frequency domain takes the form $[e^{-j\omega'_x}, e^{-j\omega'_y}, \Omega_{ct}] \in \mathbb{C}^2\mathbb{R}$.

Assume the antenna patterns are restricted to $0 < \theta < \theta_{max}$ for all ϕ. The ROS of the spectrum observed by the rectangular aperture is constrained by a cone $\omega_x^2 + \omega_y^2 = (K\Omega_{ct})^2$, as illustrated in Fig. 4(a). The LT slants the conical region of the ROS to a different direction while following the equation $(\omega'_x - \tau_x\Omega'_{ct})^2 + (\omega'_y - \tau_y\Omega'_{ct})^2 = (K\Omega'_{ct})^2$. Such a linearly-transformed spectrum for a rectangular aperture is shown in Fig. 4(b). Linear transforms can be used in different configurations, as shown in Figs. 4(c)-(d), to reduce the number of ADCs required to sample the receiver chains.

Consider the URA in Fig. 5(a). In this case the simulated ROS of the input spectrum is a frustum bounded by the light cone, as shown in Fig. 5(c)). For convenience, we assume a 2-D matrix of τ such that $\tau_{x,y} = \tau_x + \tau_y$, where (x, y) are the coordinates of each antenna location (n_x, n_y). This configuration considers four sub-arrays (one for each quadrant), defined as shown in Fig. 5(a). Four different LTs are applied to the RF signals from these sub-arrays, combined without interference, amplified and down-converted by RF chains, and sampled using ADCs as shown in Fig. 5(b).

Our simulations assumed a $M \times N$ Nyquist-spaced URA with $M = N = 32$ and $\theta_{max} = \pi/6$, which can be achieved by using gain-enhanced patch antennas [18]. The spectrum of sub-array a (red) was shifted to the second quadrant by applying delays over both rows (τ_y steps) and columns (τ_x steps) starting from the top left corner, whereas the spectrum of sub-array b (blue) was shifted to the first quadrant (on $\omega_x - \omega_y$ plane) by applying increasing delays over rows (τ_y steps) and decreasing delays over columns (τ_x steps). The spectra of sub-arrays c and d were transformed to the third and fourth quadrants, respectively. These signals can be combined by a $K:1$ combiner without spectral overlap (Fig. 5(d)) thus allowing the ADC count to be reduced by a factor of $K = 4$. ADC complexity is therefore reduced by 75%.

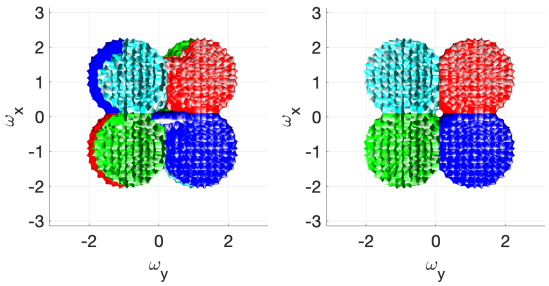

Fig. 6. Multiplexed spectra ($K = 4$) for a 16×16 URA for different mutual coupling levels C: (a) significant spectral overlaps are visible for $C = -20$ dB; and (b) no significant overlaps occur for $C = -25$ dB.

F. Effects of Antenna Coupling

Unavoidable mutual coupling between the antenna elements [19] results in inter-channel correlations that may affect multiplexing performance. Our simulations of the URA in Fig. 5(a) show that mutual coupling effects on the multiplexed spectrum can be ignored for coupling levels below -25 dB, as shown in Fig. 6. Properly-designed Nyquist-spaced arrays can offer such coupling levels, as in prior work [20], [21].

G. Hardware Implementation Issues

The required LTs can be realized by applying the LNA outputs to a set of true-time delays implemented using passive all-pass filters or transmission lines. The delayed signal components are then combined using passive power combiners (e.g., based on microstrip lines) before arriving at the ADCs. Due to the use of such low-loss delay elements, the LTs do not significantly affect receiver noise figure (NF).

However, the increase in total signal power at each ADC input requires the peak signal amplitude from each K-fold multiplexed component to be reduced by a factor of K to prevent ADC saturation, which reduces the effective number of bits (ENOB) of the digitized outputs. Specifically, multiplexing reduces each ADC's peak signal-to-noise and distortion ratio (SNDR) by $20\log_{10}(K)$ dB, such that ENOB degrades by 1-bit whenever K is doubled. Such degradation is acceptable in low-SNR scenarios, as evidenced by the popularity of low-resolution ADCs in wireless systems [22]. However, the ADC resolution must increase by $\log_2(K)$ bits for higher-SNR scenarios where SNDR must be maintained. In this case each ADC core tends to consume about K times more power [23], so the total ADC power remains constant. Nevertheless, the K-fold reduction in ADC count results in significantly lower overall system volume and power consumption by reducing the number of cables, interconnects, and power-hungry ADC buffers [24], [25] by a factor that approaches K.

III. Conclusion

This paper exploits the directional sparsity of antenna arrays to improve sampling efficiency. It proposes the use of LTs to fill the unused regions of 2D/3D spectra obtained from linear/rectangular arrays with information from multiple antennas/sub-arrays, thus reducing ADC counts for digital beamforming. ADC counts can be reduced by at least 50% for ULAs and 75% for URAs without losing degrees of freedom.

References

[1] T. S. Rappaport, J. N. Murdock, and F. Gutierrez, "State of the art in 60-GHz integrated circuits and systems for wireless communications," *Proceedings of the IEEE*, vol. 99, no. 8, pp. 1390–1436, Aug 2011.

[2] P. Busson *et al.*, "F4: Circuit and system techniques for mm-wave multi-antenna systems," in *ISSCC Proceedings*, Feb 2018, pp. 511–513.

[3] T. S. Rappaport *et al.*, "Wireless communications and applications above 100 GHz: Opportunities and challenges for 6G and beyond," *IEEE Access*, vol. 7, pp. 78 729–78 757, 2019.

[4] K. Tsutsumi *et al.*, "A 15GHz 4-channel transmit/receive RF core-chip for high SHF wide-band massive mimo in 5G," in *Silicon Monolithic Integrated Circuits in RF Systems (SiRF)*, Jan 2017, pp. 115–117.

[5] T. L. Marzetta, "Noncooperative cellular wireless with unlimited numbers of base station antennas," *IEEE Transactions on Wireless Communications*, vol. 9, no. 11, pp. 3590–3600, 2010.

[6] E. Björnson *et al.*, "Massive MIMO is a reality—what is next?: Five promising research directions for antenna arrays," *Digital Signal Processing*, vol. 94, pp. 3–20, 2019.

[7] B. Yang *et al.*, "Digital beamforming-based massive MIMO transceiver for 5G millimeter-wave communications," *IEEE Trans. Microwave Theory and Techniques*, vol. 66, no. 7, pp. 3403–3418, July 2018.

[8] L. Zhang and H. Krishnaswamy, "Arbitrary analog/RF spatial filtering for digital MIMO receiver arrays," *IEEE Journal of Solid-State Circuits*, vol. 52, no. 12, pp. 3392–3404, Dec 2017.

[9] L. Zhang and H. Krishnaswamy, "Recent advances in analog/RF interference mitigation for massive MIMO receivers," in *IEEE Intl. Midwest Symposium on Circuits and Systems (MWSCAS)*, Aug 2017, pp. 21–24.

[10] M. V. Komandla, G. Mishra, and S. K. Sharma, "Dual slant polarized cavity backed massive MIMO panel array antenna with digital beamforming," in *IEEE Intl. Symposium on Antennas and Propagation USNC/URSI Natl. Radio Science Meeting*, July 2017, pp. 1429–1430.

[11] C.-X. Mao, S. Gao, and T. Rommel, "Low-profile aperture-shared X/Ka-band dual-polarized antenna for DBF-SAR applications," in *International Workshop on Antenna Technology: Small Antennas, Innovative Structures, and Applications (iWAT)*, March 2017, pp. 104–107.

[12] Y. Li *et al.*, "Differentially fed, dual-band dual-polarized filtering antenna with high selectivity for 5G sub-6 GHz base station applications," *IEEE Transactions on Antennas and Propagation*, vol. 68, no. 4, pp. 3231–3236, 2020.

[13] A. Madanayake *et al.*, "Sampling H- & V-polarized antennas using a single ADC for digital antenna arrays by exploiting multi-dimensional signal processing RF circuits," in *IEEE International Conference on Digital Signal Processing (DSP)*, 2018, pp. 1–5.

[14] L. T. Bruton, "Three-dimensional cone filter banks," *IEEE Transactions on Circuits and Systems I: Fundamental Theory and Applications*, vol. 50, no. 2, pp. 208–216, Feb 2003.

[15] Lin Li and Ke Wu, "Integrated planar spatial power combiner," *IEEE Transactions on Microwave Theory and Techniques*, vol. 54, no. 4, pp. 1470–1476, 2006.

[16] D. E. Dudgeon and R. M. Mersereau, *Multidimensional Digital Signal Processing (Signal Processing Series)*. Prentice Hall, 1983.

[17] L. T. Bruton, "ENEL699 Multidimensional Signal Processing," 2004. [Online]. Available: http://www-mddsp.enel.ucalgary.ca/People/bruton/Enel699Main.html

[18] X. Zhang and L. Zhu, "Gain-enhanced patch antenna without enlarged size via loading of slot and shorting pins," *IEEE Transactions on Antennas and Propagation*, vol. 65, no. 11, pp. 5702–5709, 2017.

[19] H.-S. Lui, H. T. Hui, and M. S. Leong, "A note on the mutual-coupling problems in transmitting and receiving antenna arrays," *IEEE Antennas and Propagation Magazine*, vol. 51, no. 5, pp. 171–176, 2009.

[20] Y. Qian *et al.*, "Mutual coupling and mitigation in two-dimensional phased arrays based on planar quasi-Yagi antennas," in *2000 Asia-Pacific Microwave Conference. Proceedings*. IEEE, 2000, pp. 5–8.

[21] C. Wei and K.-L. Wu, "Array-antenna decoupling surfaces for quasi-Yagi antenna arrays," in *2017 IEEE International Symposium on Antennas and Propagation*. IEEE, 2017, pp. 2103–2104.

[22] J. Liu, Z. Luo, and X. Xiong, "Low-resolution ADCs for wireless communication: A comprehensive survey," *IEEE Access*, vol. 7, pp. 91 291–91 324, 2019.

[23] B. Murmann, "ADC performance survey 1997-2020," http://web.stanford.edu/ murmann/adcsurvey.html, 2020.

[24] M. Chen *et al.*, "Low-voltage low-power LVDS drivers," *IEEE Journal of Solid-State Circuits*, vol. 40, no. 2, pp. 472–479, 2005.

[25] K. Abugharbieh *et al.*, "An ultralow-power 10-Gbits/s LVDS output driver," *IEEE Transactions on Circuits and Systems I: Regular Papers*, vol. 57, no. 1, pp. 262–269, 2009.